Densification and characterisation of W–Cr–Nb alloys prepared by sintering of mechanically alloyed nanocrystalline powders

S. Telu*, R. Mitra and S. K. Pabi

Sintering of $(W_{1-x}Cr_x)_{90}Nb_{10}$ (x=0·3, 0·5 and 0·6) alloys, prepared through mechanical alloying of elemental powder blends, has been investigated. Relative density of >98% could be achieved by sintering at 1790°C for 5 h. Characterisation by X-ray diffraction, scanning electron microscopy and energy dispersive spectroscopy has shown the presence of W rich solid solution and Cr_2Nb phases in the microstructures of the sintered alloys. The densification of the W–Cr–Nb alloys is possible at relatively lower temperature due to use of nanostructured powder raw material obtained through high energy milling and liquid phase sintering promoted by the presence of Cr_2Nb having relatively lower melting point (1730°C). The matrix grain size of the sintered alloys is decreased, whereas hardness is increased noticeably with the amount of Cr_2Nb in the microstructure.

Keywords: Tungsten, W–Cr–Nb alloys, Mechanical alloying, Nanocrystalline powders, Sintering

Introduction

Development of the refractory metal based alloys is driven by the need for materials for high temperature structural applications in future defence and space aviation technologies. Among all the refractory metals, tungsten has the highest values of melting point (3420°C), Young's modulus (~407 GPa) and strength as well as the lowest vapour pressure.[1,2] At present, W and its alloys have found applications in rotors of dynamic inertial materials, stabilisers of aircraft wings, shields against X-ray and γ-radiation, containers for radioactive isotopes (e.g. Cobalt 60), armour penetrators and moulds. Moreover, the W based alloys are also used in fusion reactors as plasma targets. Although the partial pressure of oxygen inside the plasma reactors is expected to be low due to the vacuum environment, a very small amount of oxidation could significantly reduce the service life of the W based targets.[3] Besides load bearing applications, W is also used for several functional applications such as filaments in electric bulbs, cathodes in electron sources of scanning and transmission electron microscopes, as well as primary constituent of thermocouples and heating elements. Widespread elevated temperature application of the W based alloys in air or oxidising environment is not possible so far due to the poor oxidation resistance of this material.[4,5]

The high temperature applications of W and its alloys could be significantly increased by alloying with elements, which are expected to promote the formation of a protective oxide scale to prevent the environmental degradation of the base alloy. Studies performed on binary alloys of W with Ti (0–5%), Nb (0–25%), Mo (0–5%), Ta (0–15% and 25–50%), Cr (0–50%) or Zr (0–15%) as alloying element have shown that these alloys exhibit oxidation resistance superior to that of pure W.[6,7] Among these alloys, the W–Cr alloys have been found to possess the highest resistance to oxidation, and the minimum concentration of Cr required for formation of protective oxide scale is 50 at-%.[6] However, sintering of the W–Cr alloys without adding low melting sintering activators such as Pd and Ni is quite difficult,[8–10] because interdiffusion in the W–Cr alloys is very slow at high temperatures.[8] Itagaki and Yoda[11,12] have studied sintering and oxidation behaviour of the W–(28·19–46·47) at-%Cr alloys containing (0·14–2·27) at-%Pd or Ni. They have reported that Pd is more effective in enhancing the sinter density than Ni. However, the densities of the sintered W–Cr–Pd alloys have been reported to be only 58–77% of theoretical values. Another study by Lee[9] has reported about densification of 86 and 91% for ball milled elemental powder blends having compositions of W–25·3Cr–0·14Pd and W–45·4Cr–1·16Pd, respectively. Further investigations have confirmed that high temperature oxidation resistance of the W–Cr–Pd, alloys are superior to that of W–Cr–Ni alloys.[11,12] However, the presence of relatively low melting sintering activators with relatively low melting temperatures in the W-based alloys limits their high temperature capabilities by reducing their solidus temperatures.

In the present investigation, Nb has been selected for ternary alloying addition to the W–Cr alloys, because Cr and Nb can form relatively low melting (1730°C) Cr rich intermetallic phase (Cr_2Nb).[13] Thus, Nb is expected to

Department of Metallurgical and Materials Engineering, Indian Institute of Technology, Kharagpur 721302, India

*Corresponding author, email sureshteluiitkgp@gmail.com

Published by Maney on behalf of the Institute
Received 29 June 2012; accepted 18 August 2012
DOI 10.1179/1743290112Y.0000000035

act as an activator during sintering at temperatures >1730°C. Moreover, the Cr_2Nb Laves phase is known to posses high strength at higher temperatures, excellent creep behaviour and impressive oxidation resistance.[14] Hence, the W–Cr–Nb system has the potential to be considered as a high temperature liquid phase sintering system, which can be highly effective for maximising the amount of densification during sintering as well as high temperature stability. It is a well known fact that reduction of surface/volume ratio acts as the driving force for densification during sintering. Therefore, the effect of nanostructure formation on densification of the W–Cr–Nb alloys is of interest and deserves to be studied. Keeping aforementioned facts in mind, investigation has been carried out with the objectives of studying the effect of mechanical alloying on both structure of the phases in the elemental powder blends with composition of $(W_{1-x}Cr_x)_{90}Nb_{10}$ (x=0·3, 0·5 and 0·6 in at-%) and densification of their compacts through the conventional sintering route.

Experimental

Elemental powders of W (99·95% purity, 3–4 μm particle size), Cr (99·95% purity, 10–15 μm particle size) and Nb (99·95% purity, 10–20 μm particle size) were used in the present study. Three different compositions of the $(W_{1-x}Cr_x)_{90}Nb_{10}$ alloys (x=0·3, 0·5 and 0·6) were prepared via conventional sintering route. Before sintering, elemental powder blends were mechanically alloyed using high energy planetary ball mill (Pulverisette 5; Fritsch GmbH, Idar-Oberstein, Germany) in a tungsten carbide (WC) vial. The ball/powder ratio being used for milling was 10 : 1, and the milling speed was 300 rev min^{-1}. Following the process of high energy milling, the powders were charged into a uniaxial die and hydraulically pressed by applying uniaxial pressure of 350 MPa. The green compacts were then placed inside a continuous pusher type furnace (FHD Furnace Limited, Wexham, UK). Sintering was performed in H_2 atmosphere at 1790°C for 5 h.

The densities of the sintered products were evaluated by the Archimedes principle using a microbalance equipped with density measurement kit (ME235P; Sartorius, Hamburg, Germany), and the final results were averaged out of five successive measurements. A high resolution X-ray diffractometer (Philips PW 3040/60; Panalytical B.V., Almelo, The Netherlands) was used for recording the X-ray diffraction (XRD) patterns of both powders and sintered specimens. In addition, a scanning electron microscope (SEM) (Zeiss Evo 60; Carl Zeiss NTS GmbH, Oberkochen, Germany) and energy dispersive spectroscopy (EDS) (Oxford Instruments, AZtechEnergy, Oxfordshire, UK) were used for examining the microstructures of the sintered alloys and identifying their phase constituents respectively. Vickers microhardness of the sintered samples was measured by a microhardness tester (Micromet 5103; Buehler Ltd, Lake Bluff, IL, USA) operated under 200 g load for a dwell time of 15 s. Results of the hardness measurements with standard deviations were averaged out of 10 successive indentations for each test.

Results and discussion

Characterisation of ball milled powders

Peaks representing the phases present in the $(W_{0·5}Cr_{0·5})_{90}Nb_{10}$ elemental powder blend ball milled

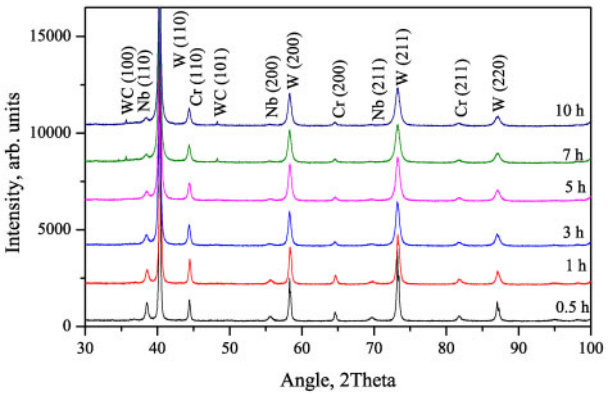

1 X-ray diffraction patterns (Cu K_α radiation) of $(W_{0·5}Cr_{0·5})_{90}Nb_{10}$ elemental powder blend after milling for different durations

for different durations are displayed in the XRD patterns shown in Fig. 1. Examination of these patterns indicates the presence of three different solid solutions enriched in W (W_{ss}), Cr (Cr_{ss}) and Nb (Nb_{ss}) phases in the elemental powders. Further, the intensities of the Nb_{ss} peaks are found to decrease with milling time, whereas the peaks of the W_{ss} are marginally shifted towards higher angle with increase in milling time. These observations indicate an increase in the lattice parameter of the W_{ss} phase, which is apparently due to the substitution of W lattice (r_W=0·139 nm) sites with larger size Nb atoms (r_{Nb}=0·146 nm). In contrast to the observations regarding Nb_{ss} and W_{ss} peaks, changes in the intensities of the Cr_{ss} peaks with milling time are found to be relatively smaller. This observation suggests that the extent of reaction of Cr with either Nb or W during ball milling is quite limited. This result is similar to that reported previously for milling of $Cr_{19}Mo_{40}W_{40}Pd_1$ elemental powders for up to 24 h.[10]

Furthermore, the XRD patterns also show continuous broadening of the W_{ss} peaks with reduction in the intensity, which may be attributed to the residual strains in the W rich phase and the refinement of the W_{ss} crystallite size in the powders subjected to ball milling. The root mean square (rms) strain and the average crystallite size of the W_{ss} phase in all three alloys have been estimated using the Voigt function (convolution of the Cauchy and Gaussian functions).[15] The results show that the rms strain in each of the ball milled powder blends increases with time of milling and reaches ~0·45% in all the investigated powder compositions subjected to milling for 10 h. As expected, a progressive decrease in the crystallite size with increase in the duration of milling is observed (Fig. 2 and Table 1). Ball milling for periods beyond 5 h has also shown a reasonable reduction in the W–Cr–Nb alloy crystallite size, as is evident from Table 1. Furthermore, examination of the results in Fig. 1 shows the absence of WC peaks in the XRD patterns from the powders milled for 0–5 h, whereas their presence is noted in the patterns representing the powders milled for 7 and 10 h. These observations confirm that milling beyond 5 h results in considerable amount of WC contamination, and quantitatively similar feature has been observed during milling of pure W.[16] Thus, in order to minimise erosion of the grinding media as well as strain hardening of the W particles, the duration of milling before sintering was

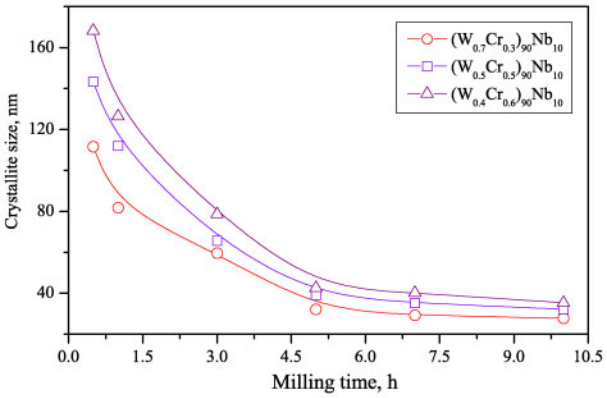

2 Plots showing variations of crystal size of W_{ss} in W–Cr–Nb elemental blends with milling time up to 10 h

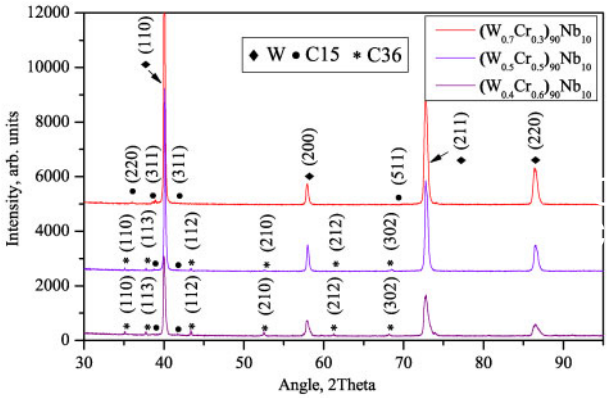

3 X-ray diffraction patterns (Cu K_α radiation) obtained from W–Cr–Nb alloys sintered at 1790°C for 5 h

restricted to 5 h in the present investigation. For the powders milled for 5 h, it may be appropriate to consider WC contamination of the alloy powders as insignificant.

Characterisation of sintered W–Cr–Nb alloys

The XRD pattern in Fig. 3 shows the presence of both W_{ss} and Cr_2Nb in the microstructure of the as sintered alloys. It has been reported[17] that formation of Cr_2Nb from elemental mixture of Cr and Nb occurs at ⩾850°C in H_2 atmosphere. Two forms of Cr_2Nb were identified by XRD analysis. The C15 structured Cr_2Nb phase (cubic with lattice parameters $a=b=c=6{\cdot}9899$ Å) has been observed in the $(W_{0{\cdot}7}Cr_{0{\cdot}3})_{90}Nb_{10}$ alloy, whereas both C15 and C36 (hexagonal with lattice parameters $a=b=4{\cdot}9670$ Å, $c=8{\cdot}0590$ Å) structures of Cr_2Nb are found to be present in $(W_{0{\cdot}5}Cr_{0{\cdot}5})_{90}Nb_{10}$ and $(W_{0{\cdot}4}Cr_{0{\cdot}6})_{90}Nb_{10}$ alloys. Both types of the Cr_2Nb phases have been also reported in the microstructures of the as cast Nb–Cr–(1–12 at-%W) alloys.[18,19] Among the Cr_2Nb phases, the high temperature Laves phase (C14) is stable above 1650°C, whereas the low temperature (C15) Laves phase is stable at temperatures below 1650°C.[14] The C14 type Laves phase is believed to transform with decreasing temperature into C15 type Laves phase through the formation of an intermediate phase with metastable C36 structure.

The SEM backscattered electron images of $(W_{0{\cdot}7}Cr_{0{\cdot}3})_{90}Nb_{10}$, $(W_{0{\cdot}5}Cr_{0{\cdot}5})_{90}Nb_{10}$ and $(W_{0{\cdot}4}Cr_{0{\cdot}6})_{90}Nb_{10}$ alloys sintered at 1790°C for 5 h are displayed in Fig. 4. Examination of these images indicates the presence of two phases having relatively brighter and darker contrasts. Typical EDS spectra gathered from relatively brighter and darker regions of the $(W_{0{\cdot}5}Cr_{0{\cdot}5})_{90}Nb_{10}$ alloy are shown in Fig. 5. Furthermore, the results obtained by EDS analysis on all three alloy samples are presented in Table 2. The standard deviation of each EDS result is also shown with the average data in this table. Examinations of the results in Fig. 5 and Table 2 indicate that the Cr_2Nb Laves phase is essentially located at grain boundaries, and the EDS spot analyses at these regions confirm the presence of nearly 6–13 at-%W as substitutional solute in the Cr_2Nb phase. This observation may be attributed to the fact that solid solubility of W is ~8 at-% in the Cr_2Nb at 1350°C, and the W atoms are expected to substitute for either Cr or Nb atoms in this intermetallic alloy.[19] The scatter in the results presented in Table 2 could be attributed to significantly larger interaction volume surrounding the area being examined through EDS in the SEM.

Table 1 Average crystallite sizes at different milling times

	Average crystallite size after milling for		
Composition/at-%	5 h	7 h	10 h
$(W_{0{\cdot}7}Cr_{0{\cdot}3})_{90}Nb_{10}$	32·1 nm	29·3 nm	27·8 nm
$(W_{0{\cdot}5}Cr_{0{\cdot}5})_{90}Nb_{10}$	38·9 nm	35·2 nm	32·3 nm
$(W_{0{\cdot}4}Cr_{0{\cdot}6})_{90}Nb_{10}$	42·6 nm	39·2 nm	35·4 nm

Figure 6 shows the isothermal section of W–Cr–Nb phase diagram at 1500°C.[20] This figure shows that position of the $(W_{0{\cdot}4}Cr_{0{\cdot}6})_{90}Nb_{10}$ alloy composition lies within the two-phase region consisting of W_{ss} and Cr_2Nb Laves phase, whereas $(W_{0{\cdot}7}Cr_{0{\cdot}3})_{90}Nb_{10}$ and $(W_{0{\cdot}4}Cr_{0{\cdot}6})_{90}Nb_{10}$ alloys are expected to have only a single phase, W_{ss} at 1500°C. However, the present experimental results have shown the presence of two-phase structure ($W_{ss}+Cr_2Nb$) in all three alloys subjected to sintering at 1790°C for 5 h. Comparison of the isothermal section of the equilibrium phase diagram for the W–Cr–Nb system at 1500°C (Fig. 6) with that at 1350°C[19] indicates that the two-phase field ($W_{ss}+Cr_2Nb$) is expanded towards the W rich side with increase in temperature. It may be noted that information on phase equilibria of W–Cr–Nb system is not available for temperatures exceeding 1500°C. Therefore, based on comparison of the isothermal sections of the phase diagrams at 1350 and 1500°C, it is inferred that all three investigated alloy compositions may possibly lie in the two-phase field ($W_{ss}+Cr_2Nb$) at 1790°C. Further experimental and theoretical work is necessary to confirm this preposition. It may be further pointed out that Cr_2Nb phase has been found to contain ~8 at-%W in solid solution,[19] which may be also responsible for shift of the boundary of the two-phase region towards the W rich side of the W–Cr–Nb ternary phase diagram.

The results of image analysis of the microstructures of the as sintered W–Cr–Nb alloys, as presented in Table 2, reveal that the amount of second phase (Cr_2Nb) increases with the concentration of Cr in the investigated alloys. The variation of the volume fraction of the Cr_2Nb phase in the investigated alloys with their relative sinter densities, grain sizes as well as Vickers microhardness is presented in Fig. 7. From the results in this figure, it is confirmed that the sintered compact of nanocrystalline W–Cr–Nb alloy powders shows impressive relative density of ~98%, which is found to increase further with the amount of Cr_2Nb in the sintered alloys

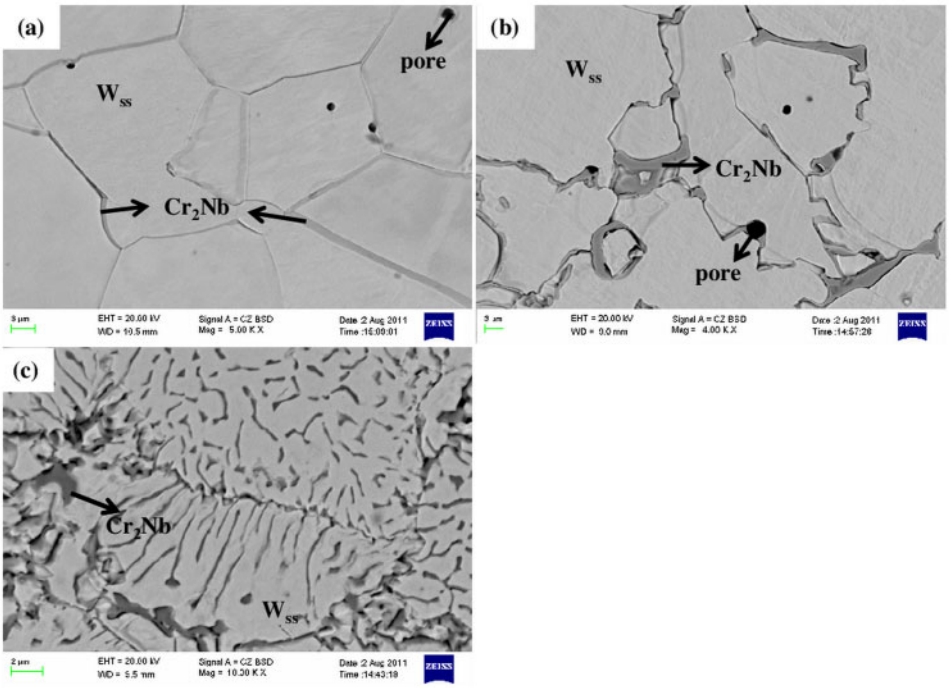

4 Images (SEM) (backscattered electron) of *a* $(W_{0·7}Cr_{0·3})_{90}Nb_{10}$, *b* $(W_{0·5}Cr_{0·5})_{90}Nb_{10}$ and *c* $(W_{0·4}Cr_{0·6})_{90}Nb_{10}$ alloys sintered at 1790°C for 5 h

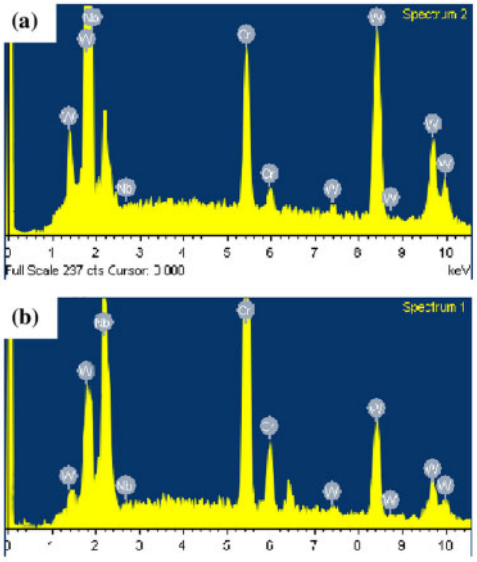

5 Energy dispersive spectroscopy spectrum from *a* brighter and *b* darker regions in microstructures of $(W_{0·5}Cr_{0·5})_{90}Nb_{10}$ alloy

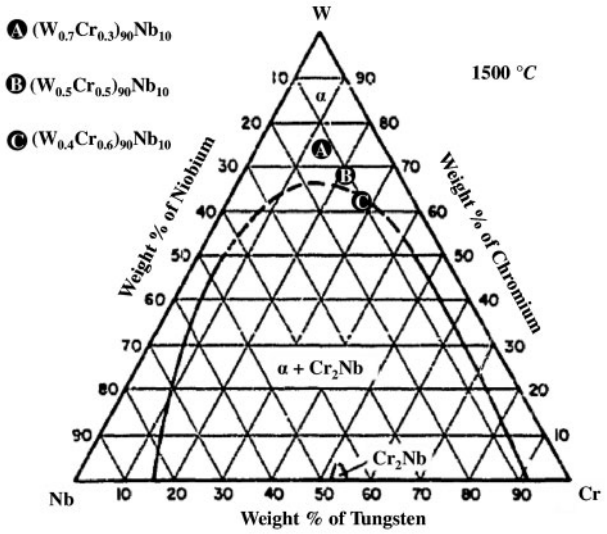

6 Isothermal section of W–Cr–Nb alloy phase diagram at 1500°C[20]

Table 2 Elemental compositions determined by EDS analysis at regions with brighter and darker contrast in microstructures of as sintered W–Cr–Nb alloys

	Brighter contrast region			Darker contrast region			
Alloy	W	Cr	Nb	W	Cr	Nb	Area fraction of Cr_2Nb phase
$(W_{0·7}Cr_{0·3})_{90}Nb_{10}$	76·5±6·45	14·8±2·32	8·70±1·33	6·21±6·91	64·5±4·97	29·3±10·81	7·62±2·72
$(W_{0·5}Cr_{0·5})_{90}Nb_{10}$	70·8±5·21	21·1±3·65	8·12±2·69	10·5±3·05	55·9±9·24	33·6±12·43	13·6±5·13
$(W_{0·4}Cr_{0·6})_{90}Nb_{10}$	65·0±7·69	27·7±6·41	7·26±4·56	8·43±2·95	65·5±8·62	26·1±6·51	28·8±3·97

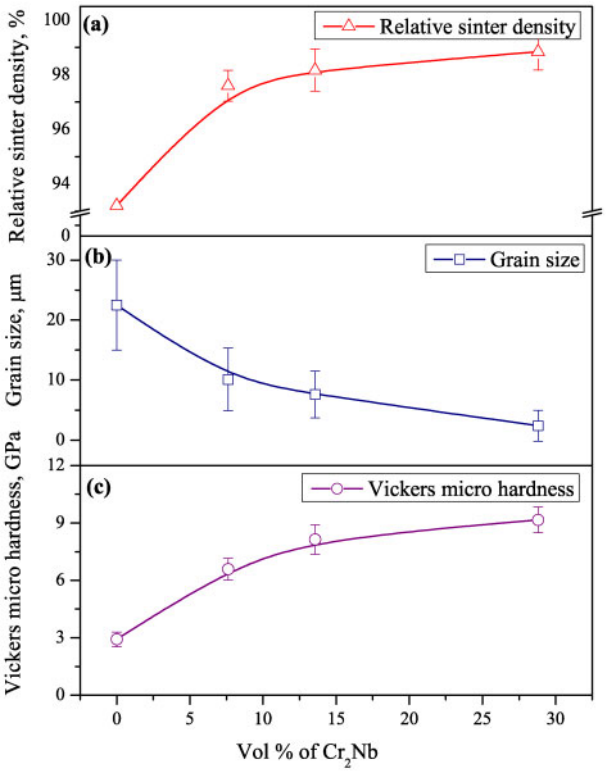

7 Relative sinter density, grain size and hardness of pure W and investigated W–Cr–Nb alloys

(Fig. 7*a*). Furthermore, the amount of densification observed for the investigated W–Cr–Nb alloys are 8–25% higher than those of as sintered pure W and W–Cr–Pd or Ni alloys.[9,11,12,16] The superior densification obtained in the present study can be attributed to two distinct reasons. First, the densification through sintering is substantially enhanced as the initial compact is made of nanostructured powders as reported in earlier studies.[16,21] Second, densification of these alloys is promoted by the formation of the intermetallic phase, Cr_2Nb, which is expected to be molten at 1790°C and thereby permit enhanced mass transport through the liquid phase. Sintering is thus activated by this liquid phase through atomic diffusion of elemental W, Cr and Nb through liquid Cr_2Nb phase wetting the metallic grains.

The average grain sizes of the W_{ss} matrix of $(W_{0·7}Cr_{0·3})_{90}Nb_{10}$, $(W_{0·5}Cr_{0·5})_{90}Nb_{10}$ and $(W_{0·4}Cr_{0·6})_{90}Nb_{10}$ alloys have been found to be 10·1, 7·6 and 2·4 μm, respectively (Fig. 7*b*). This observation shows decrease in the W_{ss} grain size with increase in volume fraction of the Cr_2Nb phase. Further, it is also evident that the sintering process employed in the present study promotes grain coarsening, such that the grain dimensions do not remain nanosize anymore. Such an observation is well expected, because in course of conventional sintering process (pressure less sintering) followed in this study, the grain growth cannot be restrained.[16,22] In addition, the large surface area of the ball milled nanostructured powders enhances the driving force for grain coarsening during sintering.[22]

The microhardness is found to increase by approximately 40%, when the volume fraction of the Cr_2Nb phase is increased from 7 to 28% (Fig. 7*c*). The reduction in grain size of W_{ss} and increase in relative density of the sintered specimens are also expected to contribute to increase in strength with increase in volume fraction of Cr_2Nb. Both increase in Cr_2Nb volume fraction and decrease in W_{ss} grain size lead to increase in obstruction to dislocation motion. Monge *et al.*[23] have observed hardness of ~2·91 GPa for pure W sintered using two-stage HIP process. On the other hand, another study on the W–Cr alloys with varying Ni content[24] has reported hardness values within the range of ~3·14–6·40 GPa. Subsequent investigations on W–Mo–Cr–Ni and W–Mo–Cr–Pd alloys have reported hardness of 4·3–6·8 GPa.[10] Thus, based on comparison with the results of earlier studies,[10,23,24] it is inferred that the hardness values obtained in the present investigation are substantially higher than those of pure W and are more or less similar to those of W–Cr alloys densified using various sinter activators.

Conclusions

The present study based on mechanical alloying followed by densification through sintering of $(W_{1-x}Cr_x)_{90}Nb_{10}$ (x=0·3, 0·5 and 0·6) alloys leads to the following conclusions.

1. The average density achieved by sintering of nanocrystalline W–Cr–Nb elemental blends at 1790°C for 5 h has been found to be >98%. The densification is promoted at relatively low temperature by both use of nanostructured mechanically alloyed powders and the formation of molten Cr–Nb phase during sintering.
2. Studies of the microstructures of the sintered samples have shown the presence of W_{ss} and Cr_2Nb phases. The amount of Cr_2Nb phase in the microstructure of the investigated alloys increases with the Cr content.
3. The W_{ss} grain size decreases, whereas the microhardness increases with increase in the volume fraction of the Cr_2Nb phase.

Acknowledgement

The authors wish to express their thanks to the Defense Research Development Organization, India, for the financial support under the project no. ERIP/ER/0700335/M/01/1014 dt.22·11·2007.

References

1. E. Lassner and W.-D. Schubert: 'Tungsten – properties, chemistry, technology of the element, alloys, and chemical compounds'; 1999, New York, Kluwer Academic/Plenum Publishers.
2. W. F. Smith: 'Structure and properties of engineering alloys'; 1993, New York, McGraw-Hill.
3. H. Bolt, V. Barabash, W. Krauss, J. Linke, R. Neu, S. Suzuki and N. Yoshida: *J. Nucl. Mater.*, 2004, **329–333**, 66–73.
4. W. W. Webb, J. T. Norton and C. Wagner: *J. Electrochem. Soc.*, 1956, **103**, (2), 107–111.
5. J. B. Berkowitz-Mattuck, A. Buchler, J. L. Engelke and S. N. Goldstein: *J. Chem. Phys.*, 1963, **39**, (10), 2722–2730.
6. G. M. Andes and R. W. Heckel: *Trans. ASM*, 1962, **55**, 193–201.
7. G. W. Titus and W. L. Clarke, Jr: *Nucl. Eng. Des.*, 1973, **24**, (1), 125–144.
8. I. Y. Dzykovich, V. V. Panichkina, V. V. Skorokhod and L. I. Shaiderman: *Sov. Powder Metall. Met. Ceram.*, 1976, **15**, (2), 151–153.
9. D.-B. Lee: *J. Less-Common Met.*, 1990, **163**, (1), 51–62.
10. S S. Diliberto, O. Kessler, C. Rapin, P. Steinmetz and P. Berthod: *J. Mater. Sci.*, 2002, **37**, (15), 3277–3284.
11. T. Itagaki and R. Yoda: *J. Jpn Inst. Met.*, 1974, **38**, (6), 486–492.

12. T. Itagaki and R. Yoda: *Trans. Natl Res. Inst. Met.*, 1975, **17**, (4), 163–169.
13. M. Venkatraman and J. Neumann: *J. Phase Equilib.*, 1986, **7**, (5), 462–466.
14. S. Hong and C. L. Fu: *Intermetallics*, 1999, **7**, (1), 5–9.
15. K. Santra, P. Chatterjee and S. Sen Gupta: *Bull. Mater. Sci.*, 2002, **25**, (3), 251–257.
16. R. Malewar, K. S. Kumar, B. S. Murty, B. Sarma and S. K. Pabi: *J. Mater. Res.*, 2007, **22**, (5), 1200–1206.
17. G. P. Khanra, A. K. Jha, S. Girikumar, K. T. Tharian and S. Kumar: *Powder Technol.*, 2010, **197**, (3), 177–183.
18. T. Takasugi and M. Yoshida: *J. Mater. Res.*, 1998, **13**, (9), 2505–2513.
19. M. Yoshida and T. Takasugi: *Mater. Sci. Eng. A*, 1999, **A262**, (1–2), 107–114.
20. J. J. English: 'Binary and ternary phase diagrams of columbium, molybdenum, tantalum and tungsten'; 1961, Columbus, OH, Defense Metals Information Center, Battelle Memorial Institute.
21. J. R. Groza: *Nanostruct. Mater.*, 1999, **12**, (5–8), 987–992.
22. V. Y. Kodash, J. R. Groza, K. C. Cho, B. R. Klotz and R. J. Dowding: *Mater. Sci. Eng. A*, 2004, **A385**, (1–2), 367–371.
23. M. A. Monge, M. A. Auger, T. Leguey, Y. Ortega, L. Bolzoni, E. Gordo and R. Pareja: *J. Nucl. Mater.*, 2009, **386–388**, (0), 613–617.
24. V. Srikanth and G. S. Upadhyaya: *J. Less-Common Met.*, 1986, **120**, (2), 213–224.